Supporting Information

Exploring the Impact of Metal Oxides Coating and Metal Atoms Doping on the Electrochemical Performance of Ni-Rich Cathode Materials

Experimental

The coated materials were created by mixing $LiNi_{0.90}Co_{0.09}Al_{0.01}O_2$ (NCA90, Gelon LIB group) with 1 mol percent M^{x+} coating material in a Nobilta-mini mechanofusion machine for 30 min while operating in a N_2 atmosphere at 5000 rpm. Note, WDXRF was also used to confirm this cathode material. The coating materials are made up of MgO (325 mesh, Sigma-Aldrich), Al_2O_3 (20 nm primary particle size, Alfa Aesar), TiO_2 (21 nm primary particle size, Aldrich), Ta_2O_5 (70-90 nm, Nanoshel), and WO_3 (100 nm particle size, Aldrich) nanopowders. The doped NCA90-based materials were created by annealing them in a tube furnace for 8 h at various temperatures (400, 600, and 800 °C) with oxygen flowing through it at a 10 sccm flow rate. Powder X-ray diffraction was used to assess the crystallographic data (XRD, Bruker New D8 Advance diffractometer). The diffraction patterns were collected with 2θ range of 10–70° using Cu Kα radiation. Using the Rietica 4.0 program, the lattice parameters and Li/Ni cation mixing were computed. It was also presummated that Li was located in site 3a, transition metals, a dopant, and extra lithium were located in site 3b, and oxygen was located in site 6c. In order to compute the amount of Ni in Li layers, a set stoichiometry for the exchange of Ni and Li had to be considered. Field-Emission Scanning Electron Microscopy (FESEM, JOEL JSM-7001F) with Energy-dispersive X-ray spectroscopy (EDX, Oxford X-max 20) and Transmission Electron Microscopy were used to capture the physical morphologies and elemental distribution images (TEM, JOEL JEM 1220).

The CR-2025 coin-type arrangement was used to conduct the electrochemical measurements. The active material's produced cathode serves as the cell's anode, and the cathode is made of lithium metal. The cathodes were made by combining active substance with carbon black (super P, Gelon LIB group), polyvinylidene fluoride (PVDF), and N-methyl-2-pyrrolidone (NMP), in the ratio of 92: 4: 4. To create the cathode sheet, the slurry was cast onto aluminum foil and cured at 120 °C. The electrode was then calendered, sliced into a disc, and loaded with a quantity of around 16–19

mg/cm^2. The electrolyte solution used for manufacturing was 1.2 M LiPF$_6$ in a 4:1 by volume percent mixture of fluoroethylene carbonate and dimethyl carbonate (DMC). The coin-type cells were created inside a glove box that contained Ar (MBRAUN UNILAB). Using the NEWARE battery tester, the electrochemical characterizations were carried out between 3.0 and 4.3 V at 30 °C. For the purpose of measuring rate capability and stability at 3.0-4.3 V, three cells were created for each sample and subjected to cycling with applied currents from C/20, C/10, C/5, C/2.5, 1C, 1.5C, and 2C rates (1C = 200 mA/g). The C/20 current was run for two cycles per 50 cycles.

All calculations reported in this work were performed by Vienna *ab initio* simulation package (VASP) [1-3] based on the periodic plane-wave density functional theory (DFT). The interaction between ion cores and valence electrons was accounted by the projector-augmented wave (PAW) [4] pseudopotentials. The exchange and correlation interactions between electrons were treated within the generalized gradient approximation (GGA) [5] with the Perdev-Burke-Ernzerhof (PBE) [6] parameterization. The additional van der Waals (vdW) contributions were obtained through the semiempirical D2 method of Grimme (DFT-D2) [7]. The effect of 3d electron correlation can be improved by considering on-site Coulomb (U) and exchange (J) interactions. On-site Hubbard term U−J values [8] of 6.2, 3.32, and 6.2 eV were applied for Ni, Co, and each dopant atoms, respectively. The cut-off energy for the expanded plane-wave basis set was set to 400 eV. The convergence thresholds for full geometry optimizations were set to 10^{-5} eV and 0.005 eV/Å for each electronic step and ionic step, respectively.

Table S1. %Weight of the transition metal in coating materials calculated from 1 mol.

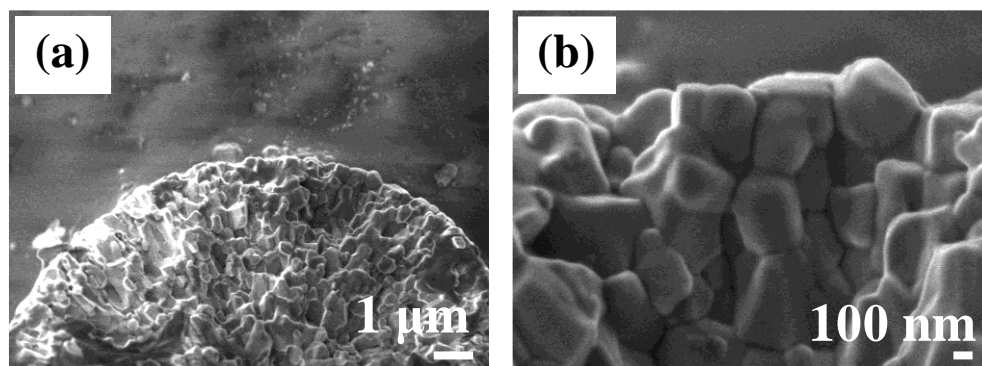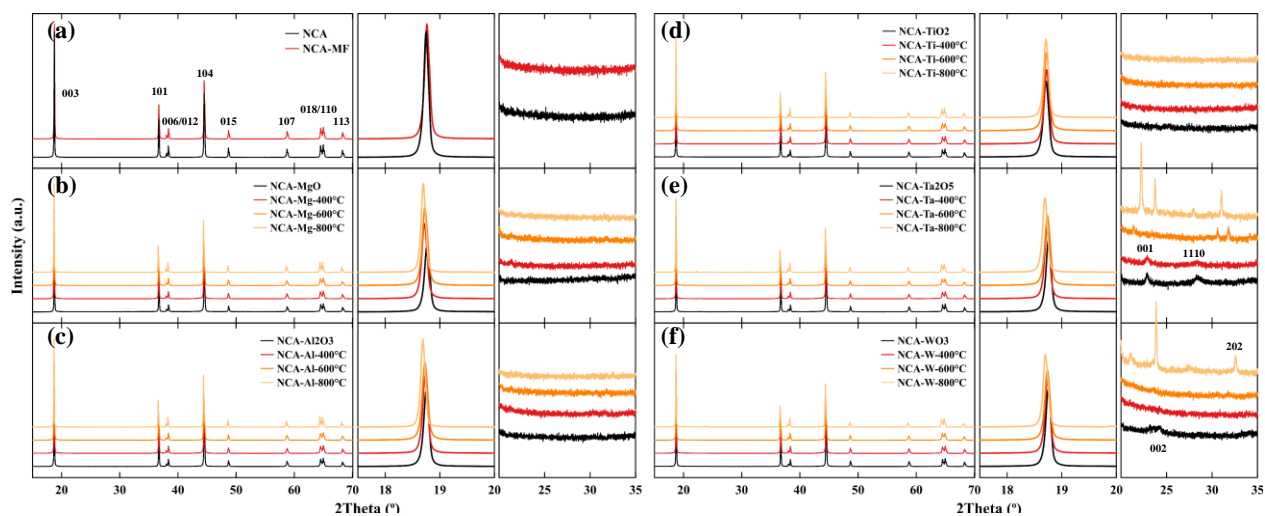| Coating material	%Weight
MgO	0.42
Al_2O_3	0.53
TiO_2	0.83
Ta_2O_5	2.28
WO_3	2.40

Fig. S1. FESEM images of pristine NCA90.

Fig. S2. XRD patterns of (a) NCA90 and mechanofused NCA90, (b) MgO coated NCA90, (c) Al$_2$O$_3$ coated NCA90, (d) TiO$_2$ coated NCA90, (e) Ta$_2$O$_5$ coated NCA90, and (f) WO$_3$ coated NCA90 with different annealing temperatures, including 400℃, 600℃, and 800℃, respectively.

Table S2. The summarized oxidation states.

Atoms	Oxidation state	Atomic radii (pm)	Ionic radii (pm)
Li	+1	167	76
Ni	+2	149	69
Ni	+3	149	56
Co	+3	152	55
Mg	+2	145	72
Al	+3	118	54
Ti	+4	176	61
Ta	+5	145	64
W	+6	193	60
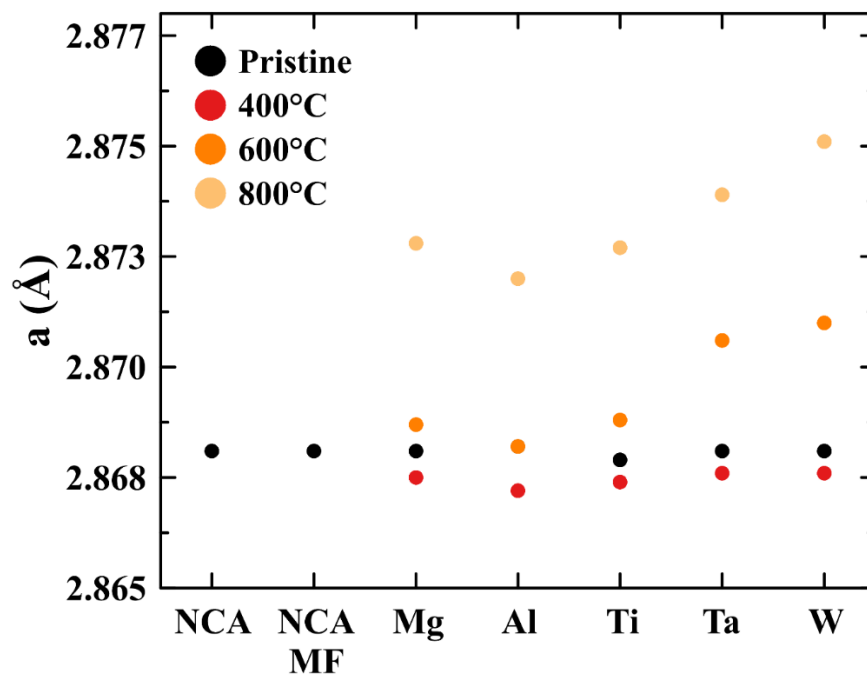
Fig. S3. The comparison between pristine NCA90, coated NCA90, and doped NCA90 of the a-lattice parameters. All lattice parameters and Li^{1+}/Ni^{2+} anti-site defects were obtained from the Rietveld refinement based on the layered $R\text{-}3m$ structure.
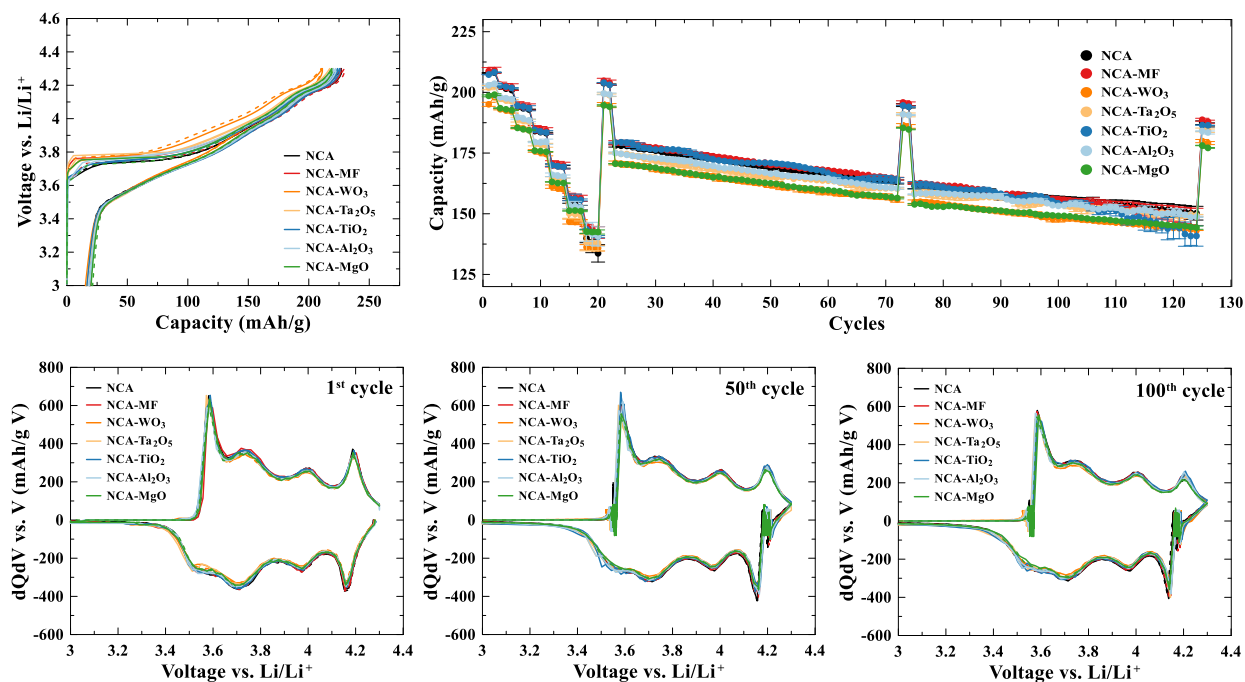
Fig. S4. The electrochemical performance of the 2032-coin cell type batteries. (a) the galvanostatic charge-discharge profiles, (b) the rate capability and the stability test, and the differential capacity as a function of voltage (dQ/dV vs. V) of the pristine NCA90 and the coated NCA90 materials at different cycles (c) 1st cycle, (d) 50th cycle, and (e) 100th cycle.
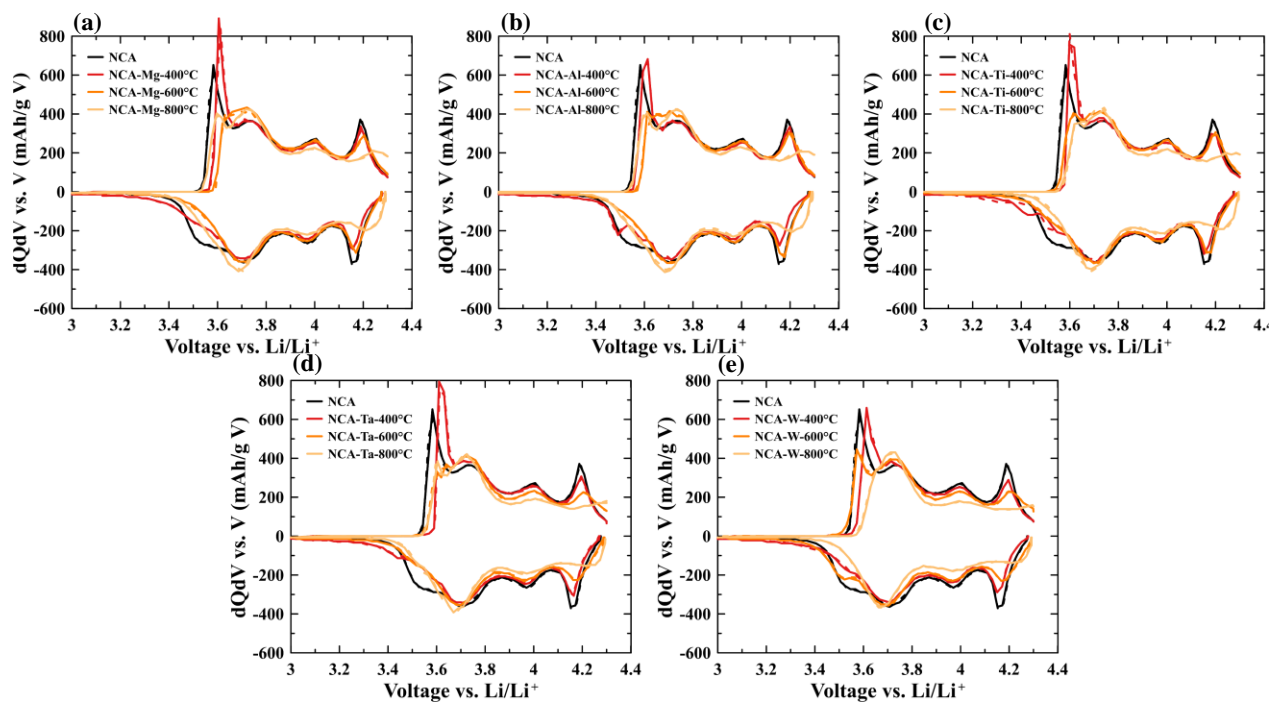
Fig. S5. The differential capacity as a function of voltage versus voltage (dQ/dV vs. V) of pristine NCA90 and the doped NCA90 prepared at the annealing temperature. (a) Mg-doped NCA90, (b) Al-doped NCA90, (c) Ti-doped NCA90, (d) Ta-doped NCA90, (e) W-doped coated NCA90.
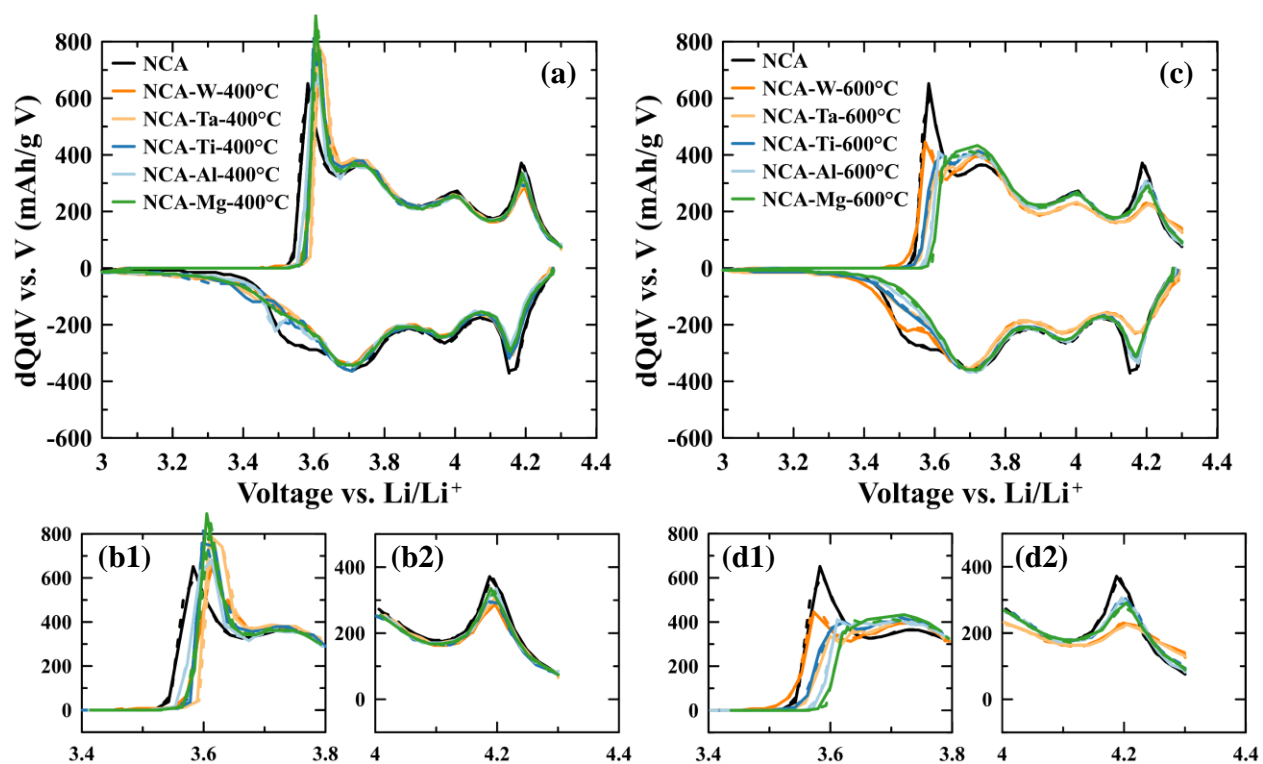
Fig. S6. The differential capacity as a function of voltage versus voltage (dQ/dV vs. V) of pristine NCA90 and the doped NCA90 prepared at annealing temperature of (a-b) 400 °C, and (c-d) 600 °C.
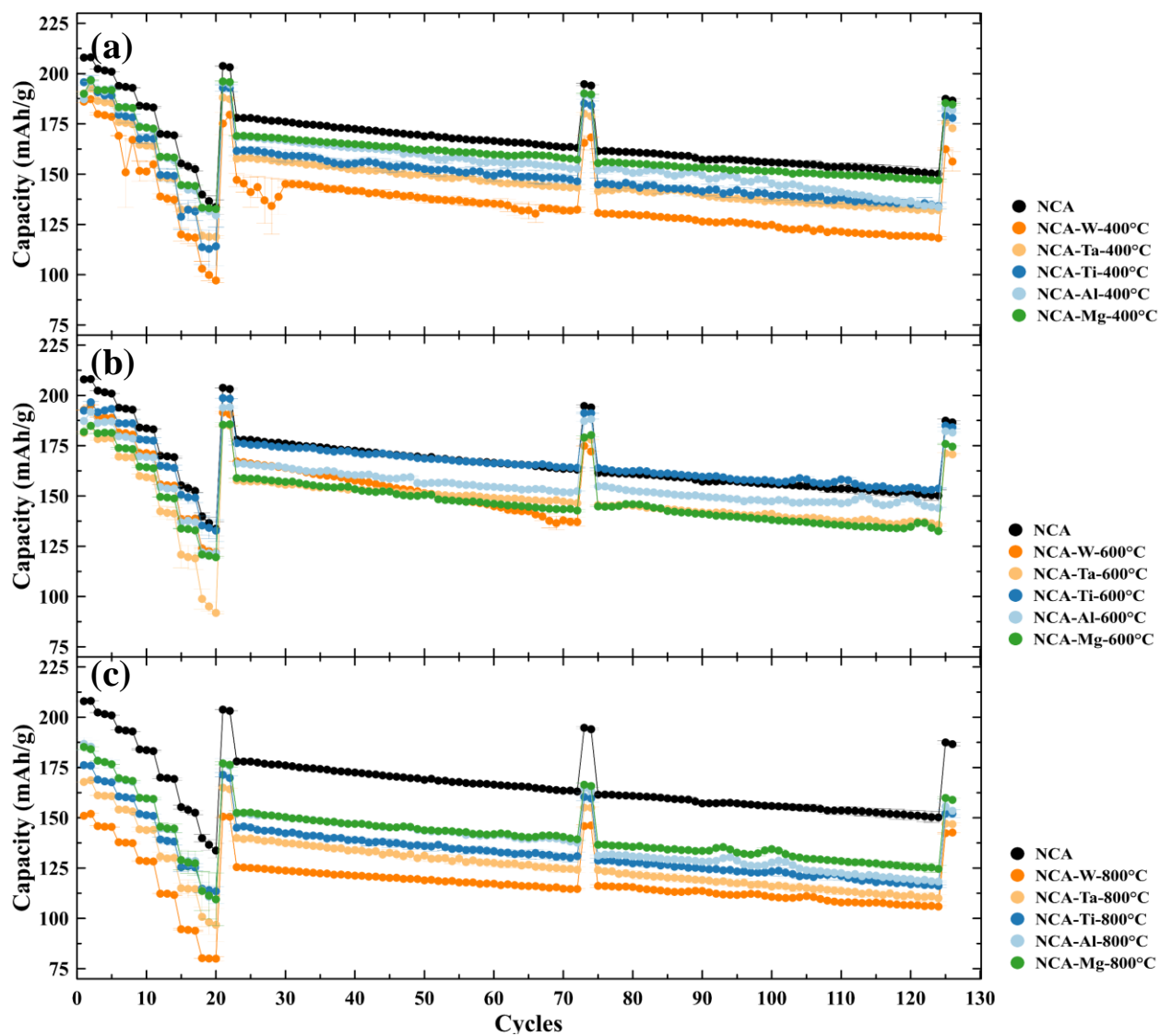
Fig. S7. The rate capability and the stability test of the pristine NCA90 and the doped NCA90 materials at the annealing temperature (a) 400 ℃, (b) 600 ℃, and (c) 800 ℃.
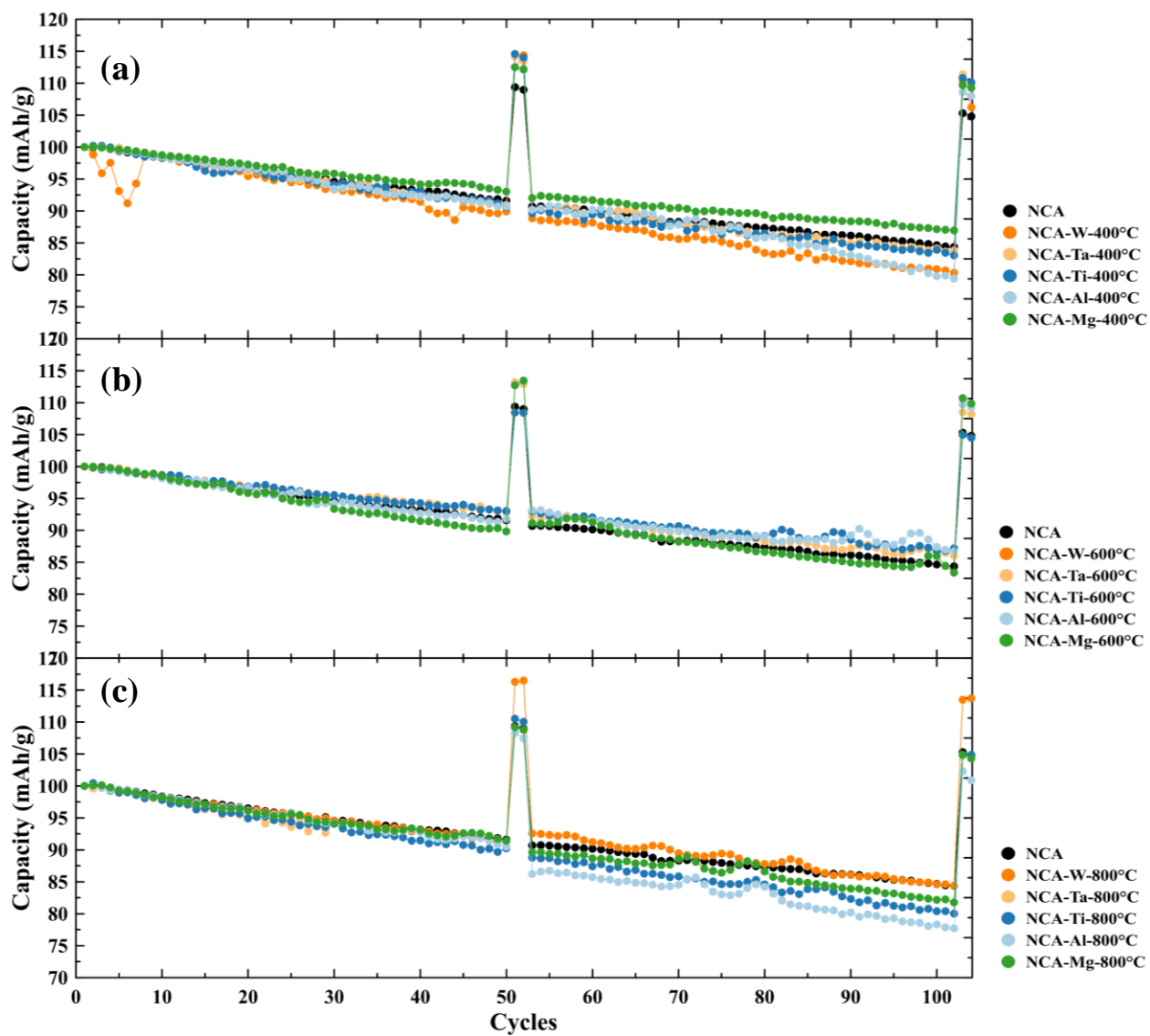
Fig. S8. The capacity retention of the pristine NCA90 and the doped NCA90 materials at the annealing temperature (a) 400 °C, (b) 600 °C, and (c) 800 °C.
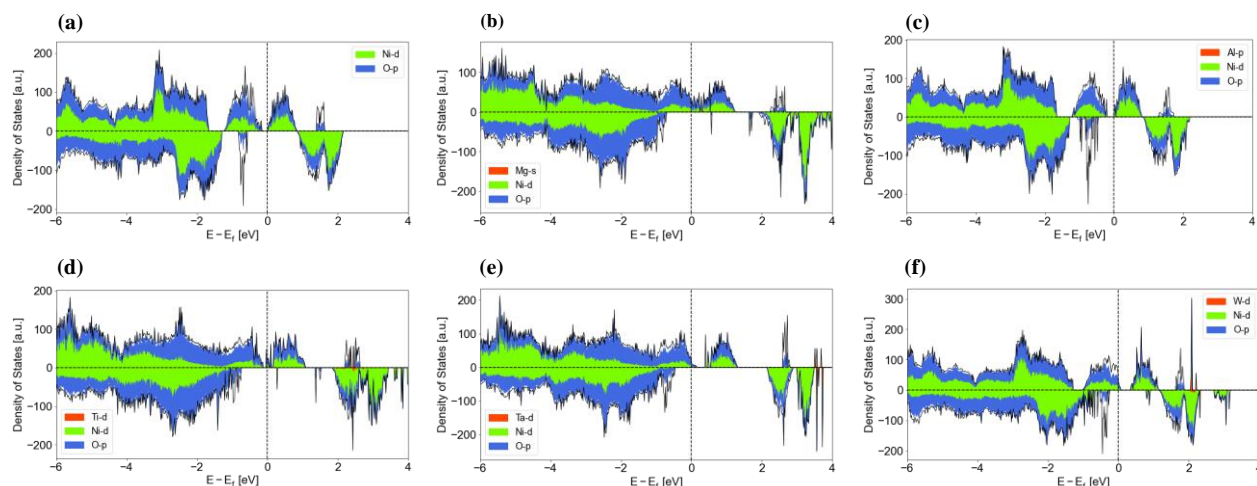
Fig. S9. The calculated density of states for the (a) pristine NCA90, (b) Mg-doped, (c) Al-doped, (d) Ti-doped, and (e) Ta-doped NCA90, and (f) W-doped NCA90.

References

1. G. Kresse and J. Hafner, *Physical Review B*, 1993, **47**, 558-561.

2. G. Kresse and J. Furthmüller, *Computational Materials Science*, 1996, **6**, 15-50.

3. G. Kresse and J. Furthmüller, *Physical Review B*, 1996, **54**, 11169-11186.

4. G. Kresse and D. Joubert, *Physical Review B*, 1999, **59**, 1758-1775.

5. J. P. Perdew, K. Burke and M. Ernzerhof, *Phys. Rev. Lett.*, 1996, **77**, 3865-3868.

6. J. P. Perdew, M. Ernzerhof and K. Burke, *The Journal of Chemical Physics*, 1996, **105**, 9982-9985.

7. G. Stefan, *Journal of Computational Chemistry*, 2006, **27**, 1787-1799.

8. V. I. Anisimov, J. Zaanen and O. K. Andersen, *Physical Review B*, 1991, **44**, 943-954.